Correspondence to:
S. A. Thaller,
scott.thaller@lasp.colorado.edu

Author Contributions:
Conceptualization: Scott A. Thaller, Laila Andersson
Data curation: Scott A. Thaller, Laila Andersson, Jasper Halekas, Marcin D. Pilinski, Matthew Pollard
Formal analysis: Scott A. Thaller
Investigation: Scott A. Thaller, Laila Andersson, Steven J. Schwartz, Marcin D. Pilinski
Methodology: Scott A. Thaller, Laila Andersson, David Newman
Resources: Laila Andersson
Software: Scott A. Thaller
Supervision: Laila Andersson
Writing – original draft: Scott A. Thaller, Matthew Pollard

Bipolar Electric Field Pulses in the Martian Magnetosheath and Solar Wind; Their Implication and Impact Accessed by System Scale Size

Scott A. Thaller[1] [ID], **Laila Andersson[1]** [ID], **Steven J. Schwartz[1]** [ID], **Christian Mazelle[2]** [ID], **Chris Fowler[3]** [ID], **Katherine Goodrich[3]**, **David Newman[1,4]**, **Jasper Halekas[5]** [ID], **Marcin D. Pilinski[1]** [ID], and **Matthew Pollard[1]** [ID]

[1]Laboratory for Atmospheric and Space Physics, Boulder, CO, USA, [2]University Paul Sabatier Toulouse III, Toulouse, France, [3]Department of Physics and Astronomy, West Virginia University, Morgantown, WV, USA, [4]Department of Physics, University of Colorado Boulder, Boulder, CO, USA, [5]Department of Physics and Astronomy, University of Iowa, Iowa City, IA, USA

Abstract The scale size of the plasma boundary region between the sheath and ionosphere in the Martian system is often similar to the gyro-radii of sheath protons, ~200 km. As a result, ion energization via kinetic structures may play an important role in modifying the ion trajectories and thus be important when evaluating the large-scale dynamics of the Martian system. In this paper, we report observations made with the MAVEN Langmuir Probe and Waves instrument of solitary bipolar electric field structures, and assess their potential role in ion energization in the Martian system. The observed structures appear as short duration (~0.5 ms) bipolar electric field pulses of ~1–25 mV/m, and are frequently observed in the upstream solar wind and inside the sheath. The study presented in this paper suggests that the bipolar electric field structures observed at Mars have an average electrostatic potential drop of ~0.07 V. The estimated upper rate at which these structures could further energize the protons is estimated, assuming the protons gain the full 0.07 eV, to be ~0.13 eV per gyration, or a change in proton energy of ~0.3%, and a corresponding change in the gyroradius of ~0.3 km. These numbers imply that to first order the bipolar structures are not a significant source of ion energization in the Martian magnetosheath.

1. Introduction

The Phobos-2 mission showed that the Martian environment is full of high frequency electromagnetic and electrostatic waves (for example, Grard et al., 1991; Mazelle et al., 2004; Nairn et al., 1991). However, their identity and importance to the system has not been fully evaluated because of the limited spectral domain data from the Phobos-2 mission. The electric field information was compressed onboard into the frequency domain, and the resulting single-point power spectra do not provide enough information to determine the detailed time domain properties of the electric field fluctuations. With the MAVEN mission (Jakosky et al., 2015) the Langmuir Probes and Waves (LPW) (Andersson et al., 2015) instrument not only provides the electric field information from onboard compression in the frequency domain, but also provides selected burst captures of the electric field in the time domain. As will be shown in this paper, a significant number of bipolar electric field solitary structures are observed at Mars. In this paper we make the first attempt to estimate the impact of kinetic scale bipolar electric field structures on ion energy and the relevance to the larger scale Martian system.

Kinetic scale bipolar electric field solitary structures have been studied computationally and in lab plasmas for over 50 years (e.g., Berk et al., 1970; Lynov et al., 1979; Morse & Nielson, 1969; Saeki et al., 1979). As the name indicates, solitary structures are non-periodic structures, which results in their being difficult to fully identify and describe without multipoint observations. Another complication for solitary structures is that the electric field signature in the frequency domain shows up as a broadband frequency response over a limited time period. Using time domain observations allows different solitary structures to be identified.

At Earth, solitary bipolar electric field structures are typically identified as either phase-space holes or acoustic solitary structures on either electron or ion scales (e.g., Franz et al., 2005; Hobara et al., 2008; Khotyaintsev et al., 2010; Main et al., 2006). Ion acoustic solitons have a potential which is positive (negative) if compressive (rarefactive), and propagate at $V_{beam} \pm c_s$, in the frame of the background plasma when excited by a beam

population at V_{beam} relative to the background plasma (Cattell et al., 1998; Lotko & Kennel, 1983). Here, c_s is the ion acoustic speed: $c_s = (k_B T_e + 3k_B T_i/m_i)^{\frac{1}{2}}$; note that when $T_e \sim T_i$ strong Landau damping of the ion acoustic mode happens; for $T_e > T_i$ or $T_i >> T_e$ the damping is modest. Where kB, mi, T_e, and T_i and the Boltzmann constant, ion mass, electron, and ion temperatures, respectively. Ion acoustic solitons have a size of $\sim 5 - \sim 10$ s Debye lengths (e.g., Dombeck et al., 2001).

Electron acoustic solitons are negative (positive) if compressive (rarefactive) electrostatic potential structures with a net potential that form in a plasma consisting of cold and hot electrons, are a few Debye lengths in scale size and propagate at the electron-acoustic speed, c_{ea}, which is intermediate between the two electron thermal velocities, $c_{ea} = \sqrt{\frac{n_{c0}}{n_{h0}}} v_{e,th}$, where $v_{eth} = \sqrt{\frac{k_B T_e}{m_e}}$ is the electron thermal speed of the hot electron population, and the densities of the hot and cold plasma are n_{h0} and n_{c0}, respectively. The component of hot plasma should be greater than $\sim 20\%$ (Berthomier et al., 2000). The presence of an electron beam results in electron acoustic solitons propagating backward relative to the beam (Berthomier et al., 2000).

Another class of solitary waves are Bernstein Greene Kruskal (BGK) mode waves, where reduced phase-space density of the particle species on trapped orbits results in a lower density of the particle species in question (e.g., Aravindakshan et al., 2021; Hutchinson, 2017). Phase-space holes typically have a predominantly symmetric electric potential, resulting in zero net potential across the structure (e.g., Hutchinson, 2017). Ion phase-space holes are a negative moving potential, propagating with speeds on the order of the ion thermal speed (e.g., Schamel, 1986), and have scale size of a few to ~ 10 of Debye length (Hobara et al., 2008). Electron phase-space holes have a size $\sim$ several Debye length (e.g., Bale et al., 1998), and propagate near the electron thermal speed, $v_{e,th}$. They typically have a small potential (< 0.1 T_e) and perturbations in the electron density of $dn_e/n_e < 0.01$, and distribution, $df(v)/f(v) < 0.2$ (Franz et al., 2005; Holmes et al., 2018).

Interactions of gyrating ions with the bipolar structure's electric field could have important implications for the particle dynamics in the Martian magnetosheath. With increased perpendicular energy the particles will increase their gyro radii. The system scale sizes of the plasma boundaries at Mars are $\sim 200–300$ km (e.g., Holmberg et al., 2019; Xu et al., 2016), can be comparable to the proton gyroradius, ~ 200 km. The propagation of the sheath protons may be modified at the plasma boundary if there is sufficient interaction with the bipolar fields.

This paper will first describe the electric field observations and how to use them to quantify the solitary structure information (Section 2). This is followed by observations and a statistical study of the characteristics of the bipolar structures (Section 3). A conclusion is thereafter provided with a discussion on the potential impact the bipolar structures have on the system (Section 4).

2. Datasets and Methodology

The MAVEN Langmuir Probe and Waves (LPW) instrument (Andersson et al., 2015) can operate in both current mode (as a Langmuir probe) and as an electric field instrument (in waves mode). The instrument is designed to operate based on a master cycle for which each master cycle consists of four sub-cycles. For the data presented in this paper the master cycle is 256 s long and all four sub-cycles are identical; they are in waves mode and the burst production is turned on.

Burst data is one of the products produced when the instrument is in waves mode and the raw electric field time series is recorded and separated into three different frequency ranges. The three different types of bursts are selected onboard to have the largest amplitudes and the memory is downlinked at a selected telemetry rate. For identification of solitary structures, the frequency range of 100–8,000 Hz is appropriate, corresponding to the medium frequency (MF) burst mode on MAVEN LPW. Each MF burst consist of 4,096 points taken over ~ 62.5 ms, independent of the master cycle length. Within a 1-min period about 5–15 MF bursts captures are received depending on the onboard automatic selection based on amplitude of the waveform. They can occur at any time and the timing of the bursts are not correlated between the three different frequency burst types.

As with any electric field waves instrument, calibrations of the measurements are made in the frequency domain resulting in a gain curve. The LPW burst mode data are in separate, short duration time-series cuts, and the user, depending on the frequency range, has to apply the calibration to the observations based on the calibration information given in Andersson et al. (2015). In this study the focus is on the frequency range of 300–8,000 Hz,

therefore the MF response calibration curve has been applied. The gain curve is applied by determining the characteristic "frequency" of the bipolar structure, namely the inverse of the structure duration, and selecting the gain corresponding to that "frequency" from the gain curve. It is important to note that care must be taken to check that the characteristic frequencies of the signals are in the passband of the filter, ∼300–8000 Hz, the range in which the gain is above the threshold value of 3 dB below the peak value (where the gain is 1). Outside of the passband the steeper slope of the frequency response will result in distortion of the bipolar signals. This can result in monopolar pulses being distorted to look like bipolar pulses, for example. In this study, we have verified that the bipolar electric field pulses have characteristic frequencies within the filter passband. The conversion from the potential between the two Langmuir probes to electric field is done using an effective distance between the sensors of 12.68 m. In addition to the gain correction, a shorting-factor correction of 1.2, corresponding to a 20% increase, is also applied to correct for the booms and spacecraft effectively shorting a fraction of the electric field.

Whether the bipolar electric fields studied herein are due to ion or electron acoustic solitons or phase-space holes, the parallel scale size of should be ∼1–10 Debye lengths (e.g., Dombeck et al., 2001; Franz et al., 2005; Hobara et al., 2008; Holmes et al., 2018), we will assume a spatial scale of ∼5 Debye lengths corresponding to ∼50 m. The fact that these structures and are being measured as the potential difference between two sensors with separation of 12.68 m, or ∼1/4 the bipolar structure size will introduce an error. Analysis using an analytical expression for the potential and electric field of bipolar structures, comparing the continuous electric field versus that calculated as the potential differences between points with finite separation, indicate that for the range of Debye lengths in the current study, 6.3–11.9 m, the measured peak electric field amplitude will be between 0.57 and 0.82 lower than the actual, corresponding to errors between 43% and 18%, respectively. When these two electric fields are integrated and the resulting potentials compared, the potential depth of bipolar structure will be a factor of 0.74–0.91 smaller than the actual. The electric field measurements also have an error of ∼20%, based on the Langmuir Probe boom attitudes relative to the undisturbed plasma (e.g., that the booms are not in the spacecraft wake) and how quickly the local plasma environment is changing. This latter error of ∼20% is computed by the data processing routines and is stored in the LPW MF burst data files.

The bipolar electric field pulses were identified individually, by examining by eye the LPW level 2 (L2) electric field Medium Frequency (MF 100–8,000 Hz) burst captures for bipolar pulses. The electric field is one-dimensional, along the separation of the two sensors, which in the spacecraft coordinate system is the *y*-axis. The single ended potential measurements from the two Langmuir probes are only reported at a ∼1 s cadence. In the burst mode, the electric field data combines the measurements from the two Langmuir probes onboard before being telemetered down. Since we do not have the single ended potentials at the burst cadence, we cannot directly infer the propagation direction or speed of the bipolar structures. As a result, while we clearly observe the pulse sequence, for example, positive electric field followed by negative or vice versa, we do not know if, for example, the positive phase of the bipolar pulse is caused by a positive charge propagating along the positive-y direction or a negative charge propagating along the negative-y direction. Determining the potential requires knowledge of the speed of the structures. Since the four types of bipolar structures potentially relevant to this study, described above, all have scale sizes on the order of ∼1 – ∼10 Debye lengths, we will assume a size of 5 Debye length, calculated from the particle moments described below, and divide that length by the duration of the bipolar field structure observation. In the way just described we provide a rough estimate of the speed with which to convert from the temporal to spatial domain and estimate the potential of the structures. The duration of the bipolar electric field structures used here are the time durations taken for the whole structure to pass over the spacecraft. This duration is determined by eye as the difference between the times at which the structure end and begins. The uncertainty in the determination of temporal duration due to smaller fluctuations in the electric field is ∼15%–20%.

For calculation of the Debye length, the plasma electron temperature measured by the Solar Wind Electron Analyzer (SWEA) (Mitchell et al., 2016) and ion density, assumed equal to the electron density via quasi-neutrality, measured by the Solar Wind Ion Analyzer (SWIA) (Halekas et al., 2015) are used. The SWIA density moments are accurate to ∼3% when the plasma is mainly protons (Halekas et al., 2015). We estimated the uncertainty on the SWEA electron temperature by comparing the values for temperature determined from the moment calculation to those from a Maxwell-Boltzmann fit to be ∼11% on average (the individual errors ranged from ∼2% to ∼17%). Propagating these errors, we find an error of ∼6% in the Debye length. SWIA also provides the ion temperature and bulk flow speed measurements. The magnetic field is measured by the magnetometer (MAG)
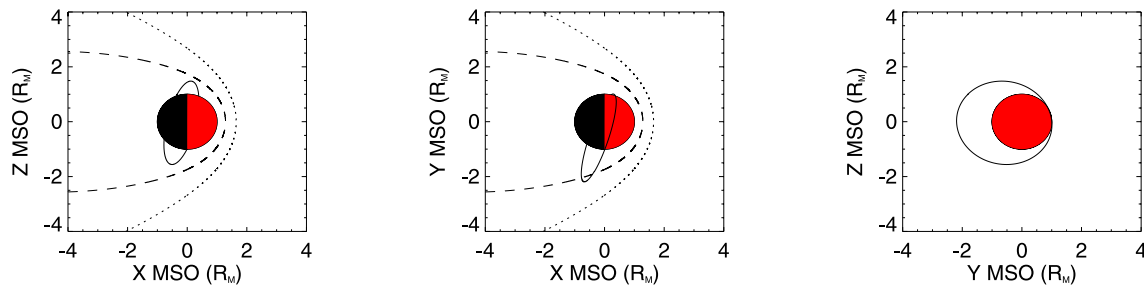
Figure 1. Three aspects of the MAVEN orbit (solid black ellipses) in Mars Solar Orbital (MSO) coordinates on 25 May 2020. The sheath is located between the dashed line (pileup boundary) and the dotted line (bow shock) defined by the Vignes et al. (2000) statistical locations.

(Connerney et al., 2015). And the presence of heavy ions is indicated by the Suprathermal and Thermal Ion Composition (STATIC) instrument (McFadden et al., 2015).

3. Observations and Results

We examined the LPW MF burst data for several days per month during May to August (inclusive) 2020, which are representative of the occurrence level of bipolar field structures for several days before and after. During this time period, the close proximity of Mars to Earth allowed for larger quantities of burst data to be telemetered back, providing routine burst waveforms. In late May 2020, MAVEN's orbit was oriented such that its apoapsis was primarily in Mars' sheath. By late August 2020, the orientation of MAVEN's orbit had apoapsis in the solar wind. This time period was also that leading up to Mars perihelion. The closer proximity of Mars to the Sun during perihelion is known create a more extended hydrogen exosphere (e.g., Halekas, 2017; Yamauchi et al., 2015). The exosphere is ionized by EUV radiation or charge exchange (e.g., Yamauchi et al., 2015). The newly created ions are initially nearly stationary in the Mars frame before being accelerated by the solar wind convection electric field resulting in the formation of a pickup ion plume (Dong et al., 2015). Both the newly created ions and plume ions appear beam-like in the frame of the solar wind. A beam population is known to be able to give rise to numerous plasma instabilities (e.g., Fuselier et al., 1987; Gary, 1991; Sauer & Dubinin, 2004) and is a relevant condition for the generation of the bipolar structures associated with acoustic solitons and phase-space holes (e.g., Crumley et al., 2001; Lefebvre et al., 2010; Main et al., 2006).

3.1. 25 May 2020 Case

The first interval we discuss occurs on 25 May 2020. In this interval MAVEN passes through the sheath near the dawn flank as shown in Figure 1. Though not captured by the statistical location of the bow shock in Figure 1, there appears to be a ∼30-min encounter with a fairly disturbed foreshock-like solar wind plasma from ∼14:40 UT to ∼15:10 UT, visible in Figure 2. Near Mars, the plasma environment just outside the bow shock consists of both solar wind plasma and a cold population of exospheric ions.

Figure 2 shows an overview plot of data collected over the orbit studied on 25 May 2020. The vertical black lines mark the burst capture times when bipolar electric field pulses are observed. These are short duration, ∼0.5 ms, bipolar electric field pulses with amplitudes along the measurement axis of ∼1–20 mV/m observed in the LPW burst captures, as described above. An example of the bipolar electric field structures observed is shown in Figure 3.

3.2. 25 July 2020 Case

The second interval examined occurs on 25 July 2020. During this period bipolar electric field structures are observed as MAVEN passes through the sheath on the dayside as shown in the orbit plots in Figure 4.

Figure 5 shows an overview of the orbit segment studied on 25 July 2020. The black vertical lines mark the times when bipolar fields are observed in the burst captures. MAVEN encounters the plasma environment outside the bow shock, consisting of the solar wind and cold exosphere ions, from about ∼14:20 to ∼15:15 UT.
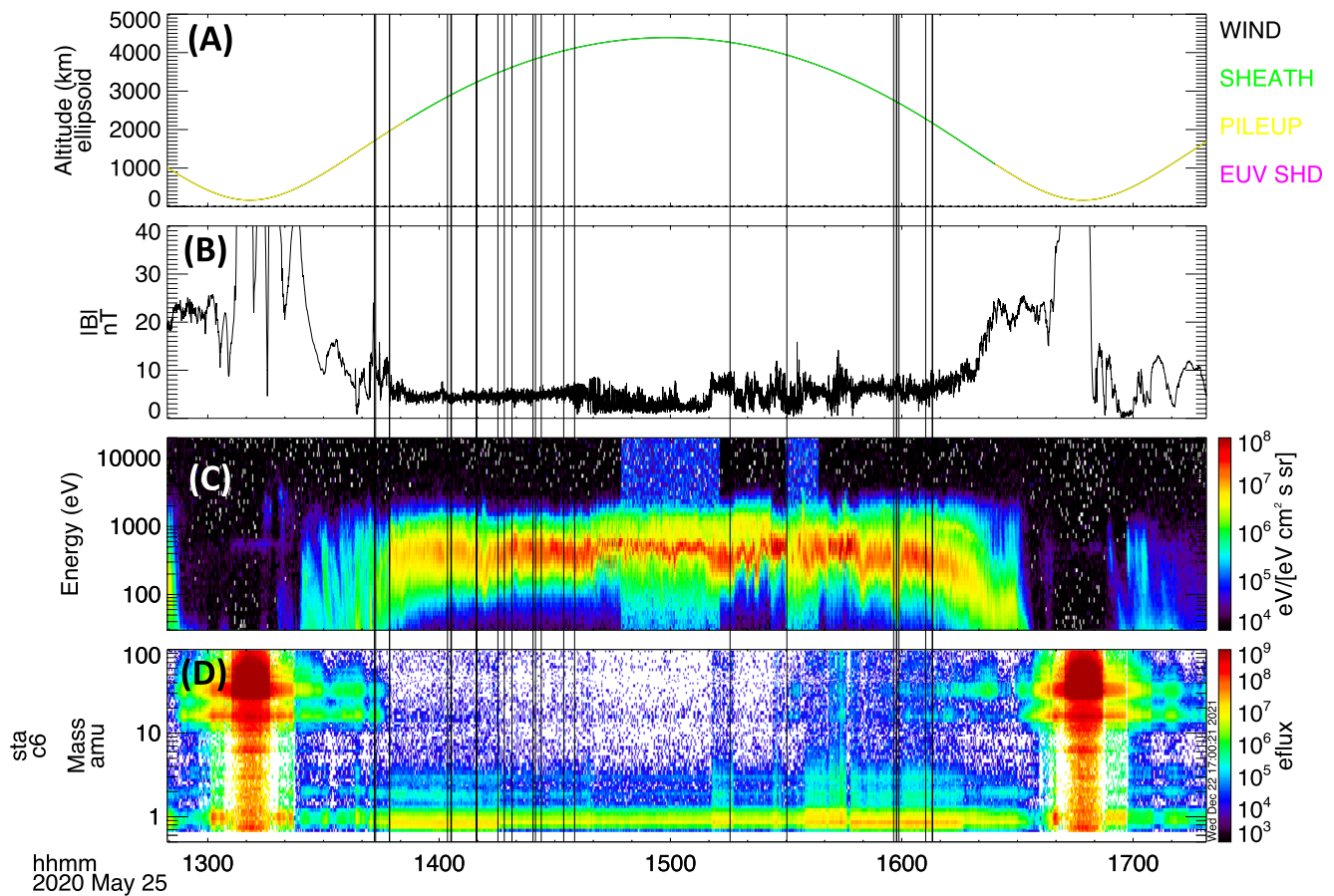
Figure 2. Overview of the 25 May 2020 interval with the location/times where bipolar electric field pulses are observed in Langmuir Probes and Waves (LPW) medium frequency bursts marked with vertical black lines. (a) is the MAVEN altitude color coded to indicate the plasma region according to a statistical study (Trotignon et al., 2006). The statistics suggest a majority of the interval is in the sheath (green), the yellow trace is the statistically determined pileup region where the magnetic field piles up on the planetary ionosphere. (b) is the magnetic field magnitude, measured by MAG, in (c) is the SWIA energy spectra, and in (d) is the STATIC ion mass spectra.

In both the 25 July and 25 May observations, the bipolar field structures are sometimes observed concurrent with strong oscillations of the magnetic field. The resulting oscillations of the background magnetic field about the spacecraft y-axis, the axis along which the LPW booms are separated, provides the opportunity to study the propagation of these bipolar structures. If the series of bipolar fields are all due to the same type of bipolar polarity (e.g., have the same charge), and are all propagating along the magnetic field in the same direction, then, when the magnetic field changes direction across the line of separation between the two Langmuir probes (the y-axis), the pulse polarity sequence should change as well; Figure 6, using the hypothetical parallel electric field of an ion phase space hole, illustrates this.

The pulse polarity reversal with the change in magnetic field orientation described above is observed, and an example interval of this is shown in Figure 7. Both acoustic solitary structures (e.g., Vasko et al., 2017) and phase space holes (e.g., Hutchinson, 2017) propagate along the background magnetic field, and we observe evidence that the bipolar structures described in this study propagate along the background magnetic field as well.

3.3. 21 August 2020 and the Statistical Examination of Bipolar Electric Fields

In late August 2020, compared to the two periods studied above, MAVEN's orbit has a longer duration in the solar wind, as can be seen in orbit plots shown in Figure 8. An overview of one and ~3/4 orbits is presented in
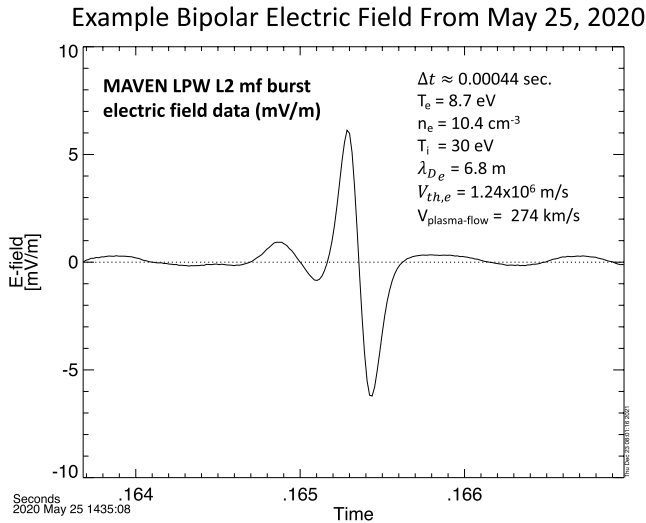
Figure 3. Example of a bipolar electric field pulse observed in MAVEN Langmuir Probes and Waves (LPW) medium frequency burst capture on 25 May 2020 near 14:35 UT. The plasma electron temperature and density are determined from SWEA and SWIA measurements, respectively, the ion temperature and bulk flow speed determined from SWIA measurements, and parameters calculated from these, used in the analysis of this structure, are called out on the plot.

Figure 9. The vertical black lines indicate the times where bipolar electric fields have been identified.

As can be seen in Figure 9, this interval includes both the sheath and the plasma environment outside the bow shock, consisting of the solar wind and cold exosphere ions. This time period has a higher rate of bipolar field observations than do the two examined above. For the three intervals examined, the lower bound of the average rate of burst captures with bipolar field observations, in the regions where bipolar fields are observed, are ∼0.28, ∼0.57, and ∼1.6 min^{-1} for May, July, and August respectively. This increase in the rate may be because this progression of time corresponds to the approach to perihelion, where the exosphere is more extended, and may provide a stronger beam-solar wind interaction for the generation of the bipolar structures. For the present examination we will use this period of higher bipolar field occurrence rate to estimate the impact these structures may have on the plasma.

We estimate the electric potential associated with the bipolar fields between the start of the structure and the midpoint where the electric field passes through zero by assuming they are ∼5 Debye length total width, a scale typical of these structures as discussed above, and using their temporal duration to estimate their speed. We then use this speed to convert from the time to the spatial domain, and spatially integrate the electric field. Due to the rough estimate of the structure size these potentials are only rough approximations. As described above, the spatial scales of bipolar structures are typically ∼1 – ∼10 Debye length; thus, we chose 5 Debye length as an estimate, but given the characteristic range of ∼1–10 Debye length, we attribute an error of a factor of ∼2 to the sizes, and hence to their speed and potential. Note, the shorting factor and gain corrections have been applied to the electric fields prior to the calculation of the potential. The asymmetries in the observed bipolar structures, and thus in the potential drop across the whole structure, could be due to either the convolution of the measured components of the parallel and perpendicular electric field, as described in more detail below, or due to a real asymmetry in the plasma structure. An example of the bipolar field and corresponding potential from the integration is shown in Figure 10.

The angle between the booms and magnetic field also needs to be considered. The one-dimensional electric field measurement is a convolution of part of the parallel electric field with part of the perpendicular electric field. This can be shown by starting with the expression for the potential of such a structure in cylindrical coordinates with z the distance along the magnetic field and r the radial distance, given by Equation 1

$$\Phi(r, z) = \Phi_0 \exp\left(-\frac{r^2}{2L_\perp^2}\right)\exp\left(-\frac{z^2}{2L_\parallel^2}\right),$$

(1)
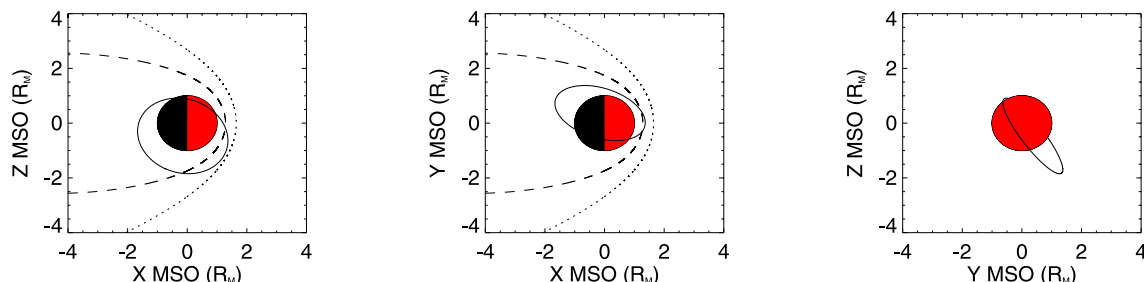
Figure 4. MAVEN orbit for 25 July 2020 from three different perspectives in Mars Solar Orbital (MSO) coordinates. MAVEN's orbit mainly passes through the sheath on the dayside according to the Vignes et al. (2000) statistical study.
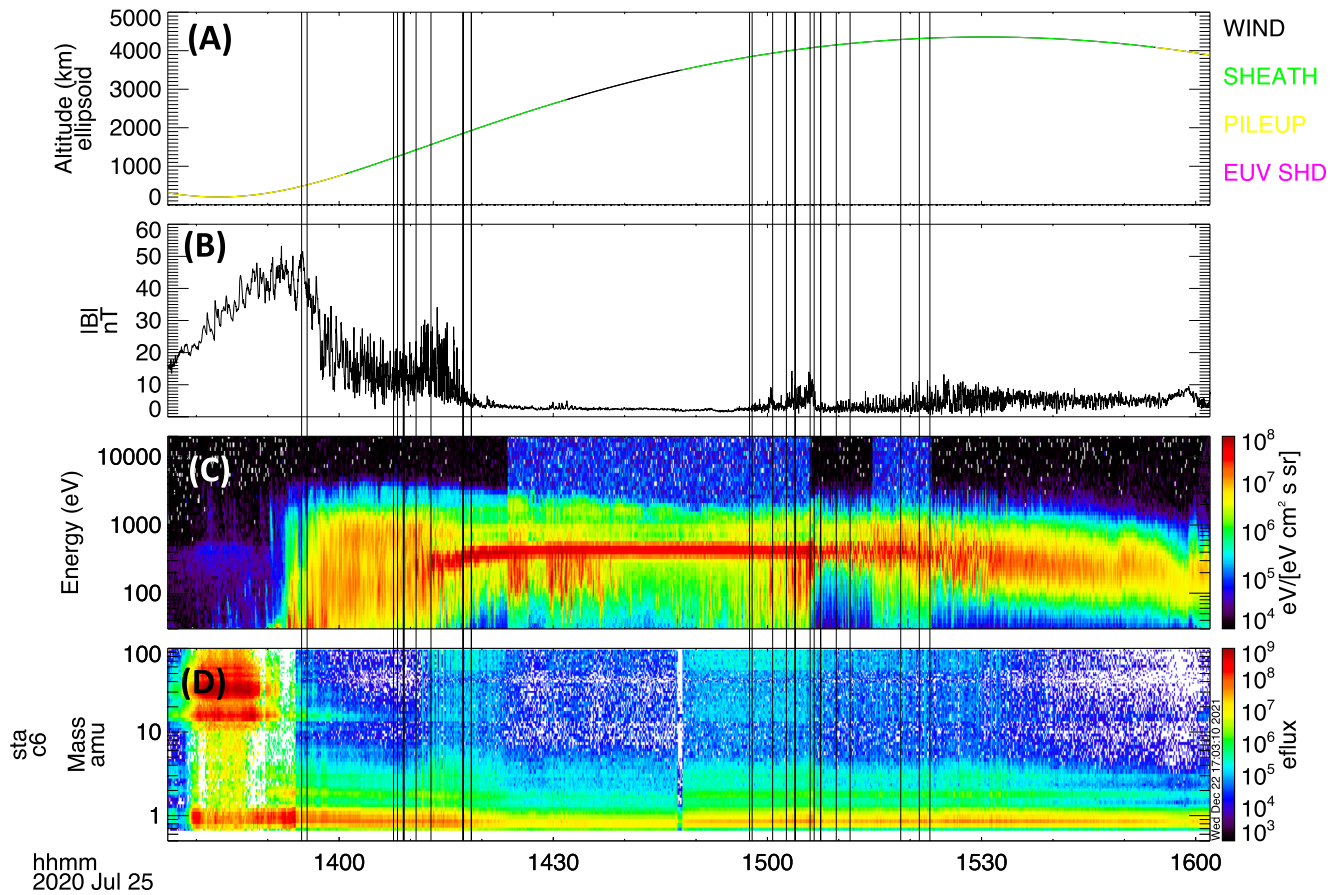
Figure 5. Overview plot of 25 July 2020 event. Same format as Figure 2. Black vertical lines mark the times that bipolar electric field pulses are observed in the Langmuir Probes and Waves (LPW) medium frequency burst waveform capture data. (a) is the MAVEN altitude color coded to indicate the plasma region according to a statistical model, (b) is the MAG magnetic field magnitude, (c) is the Solar Wind Ion Analyzer (SWIA) energy spectra, and (d) is the STATIC ion mass spectra.
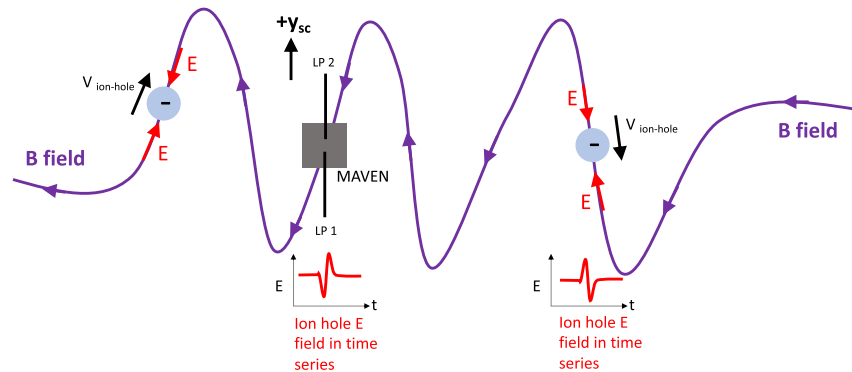
Figure 6. Cartoon illustrating how bipolar structures of the same type (polarity) propagating in one direction relative the magnetic field, can lead to either pulse polarity sequence observed by MAVEN Langmuir Probes and Waves (LPW). In this illustration ion holes propagating along the magnetic field from one direction (from the left) can be observed with either polarity depending on how the magnetic field happens to be oriented with respect to the line of separation of the two Langmuir Probes (LP1 and LP2), which is along the y-axis in spacecraft coordinates. The resulting pulse polarity sequences for two orientations are shown in the small insert plots of electric field as function of time.
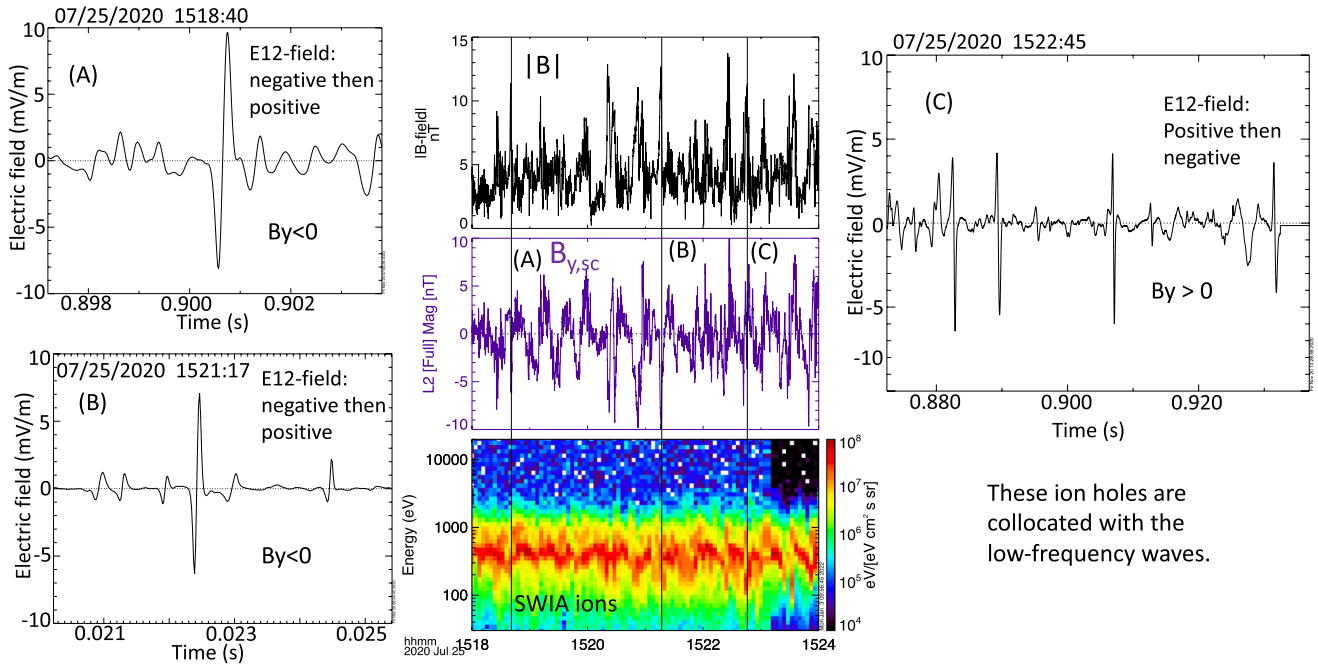
Figure 7. Three burst captures showing bipolar electric field structures are shown in panels (a–c). The corresponding time of these bipolar pulses are shown in the middle panel by the vertical lines. The polarity changes sequence with the change in the orientation of the magnetic field with respect to the Langmuir Probes and Waves (LPW) booms.

(e.g., Andersson et al., 2009; Holmes et al., 2018), where $L_\perp$ and $L_\parallel$ are the perpendicular and parallel scale sizes. Finding the total electric field, we get:

$$E = -\nabla\Phi(r,z) = \Phi(r,z)\frac{r}{L_\perp^2}\hat{r} + \Phi(r,z)\frac{z}{L_\parallel^2}\hat{z} \tag{2}$$

As the bipolar structure moves along the magnetic field, finding the potential from integrating the full electric field would use the dot product of the structure's velocity, v_{BP}, with the electric field, picking out the z component. In the present case, the one-dimensional electric field measurement made at the angle between the axis of the LPW boom separation and the magnetic field, θ, involves both parallel and perpendicular components, so that the measured 1D electric field, E_m, is:

$$E_m = \Phi(r,z)\frac{r}{L_\perp^2}\sin(\theta) + \Phi(r,z)\frac{z}{L_\parallel^2}\cos(\theta) \tag{3}$$

When this field (e.g., E_m) is integrated along the z direction, the resulting potential likewise involves a combination of parallel and perpendicular components;
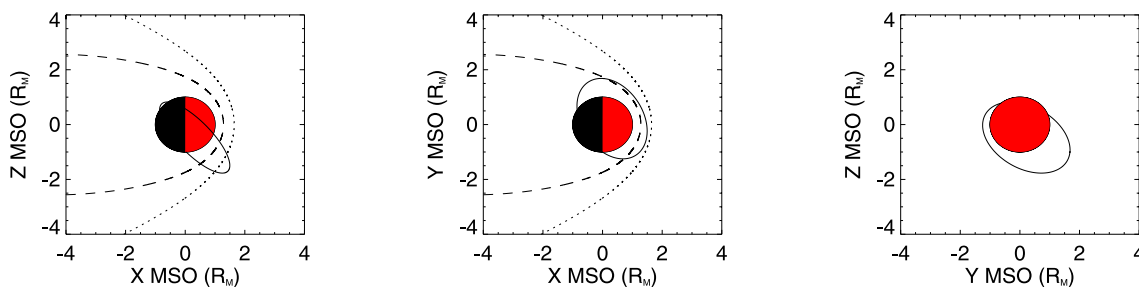
Figure 8. MAVEN orbit configuration for 21 August 2020. The orbit had a longer segment in the solar wind relative to the July and May cases described above.
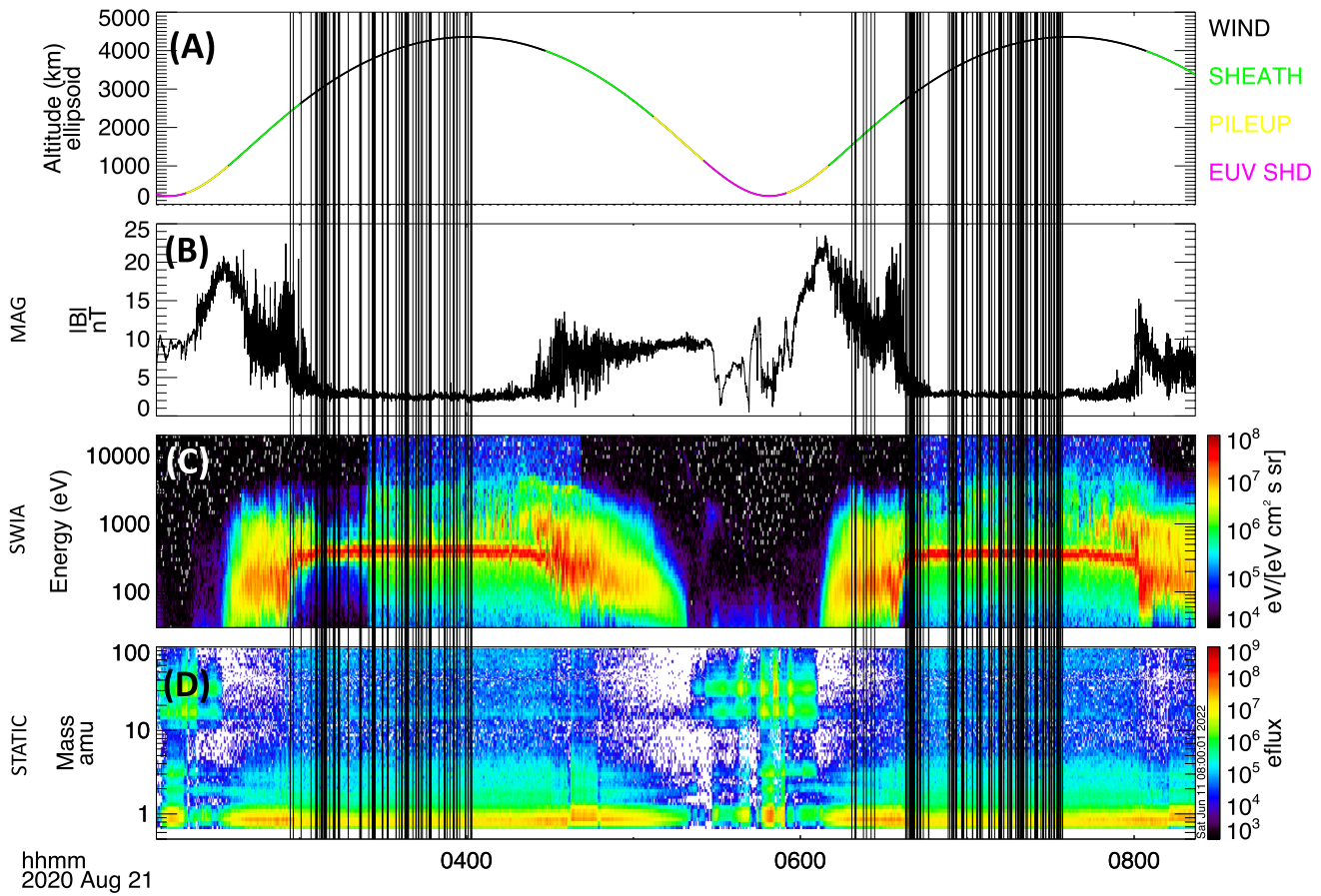
Figure 9. A period of approximately one and ∼3/4 MAVEN orbits from ∼2:00 to ∼8:00 UT on 21 August 2020. (a) is the MAVEN altitude color coded to indicate the plasma region according to a statistical model, (b) is the MAG magnetic field magnitude, (c) is the Solar Wind Ion Analyzer (SWIA) energy spectra, and (d) is the STATIC ion mass spectra. The vertical black lines indicate the times there the Langmuir Probe and Waves (LPW) MF burst captures contain bipolar electric field structures.

$$\int_0^\infty E_m v_{BP} dt = \Phi_0 \exp\left(-\frac{r^2}{2L_\perp^2}\right)\cos(\theta) + \sqrt{\frac{\pi}{2}}\frac{rL_\parallel}{L_\perp^2}\Phi_0 \exp\left(-\frac{r^2}{2L_\perp^2}\right)\sin(\theta) \tag{4}$$

Graphical examination of how the relative shape (e.g., $L_\perp$ vs. $L_\parallel$) of the structure should affect the symmetry of the bipolar pulse (not shown) suggests those observed here should be approximately spherical, for example, $L_\perp \sim L_\parallel$. We assume a $L_\parallel \sim 2.5\lambda_{De}$ based on the literature as described above. The average radial distance that the spacecraft should be from the structure's center, r, based purely on geometric consideration (e.g., the average distance of the points in a random scatter in a circle from the circle's center), is 2/3 of the radius (Stone, 1991), so that we approximate $r \sim \frac{2}{3}L_\perp$. Applying $L_\perp = L_\parallel$ and $r = \frac{2}{3}L_\perp$ we can write Equation 4 as:

$$\int_0^\infty E_m v_{BP} dt = \Phi_0 \cos(\theta) 0.8\left(1 + 0.83\tan(\theta)\right) \tag{5}$$

Where the term $\cos(\theta)0.8(1 + 0.83\tan(\theta))$ ranges from 0.8 for 0° to 0.66 for 90°. Thus, for statistical purposes, we find a relatively simple correction to the potential that accounts for the partial measurement of the electric field and the convolution of its components. Figure 11 shows the scatter plot of 235 bipolar fields observed on 21 August 2020 at the locations indicated by the vertical black lines in Figure 9. Figure 11a shows the peak electric field amplitude plotted against the duration of the bipolar pulse. The bipolar pulses range from a few tenths of an mV/m to ∼25 mV/m, and are ∼0.3–3 ms duration. Figure 11b shows the estimated potential plotted against the duration. The estimated potentials range from ∼0.002 to ∼2 V. The average estimated potential of the bipolar
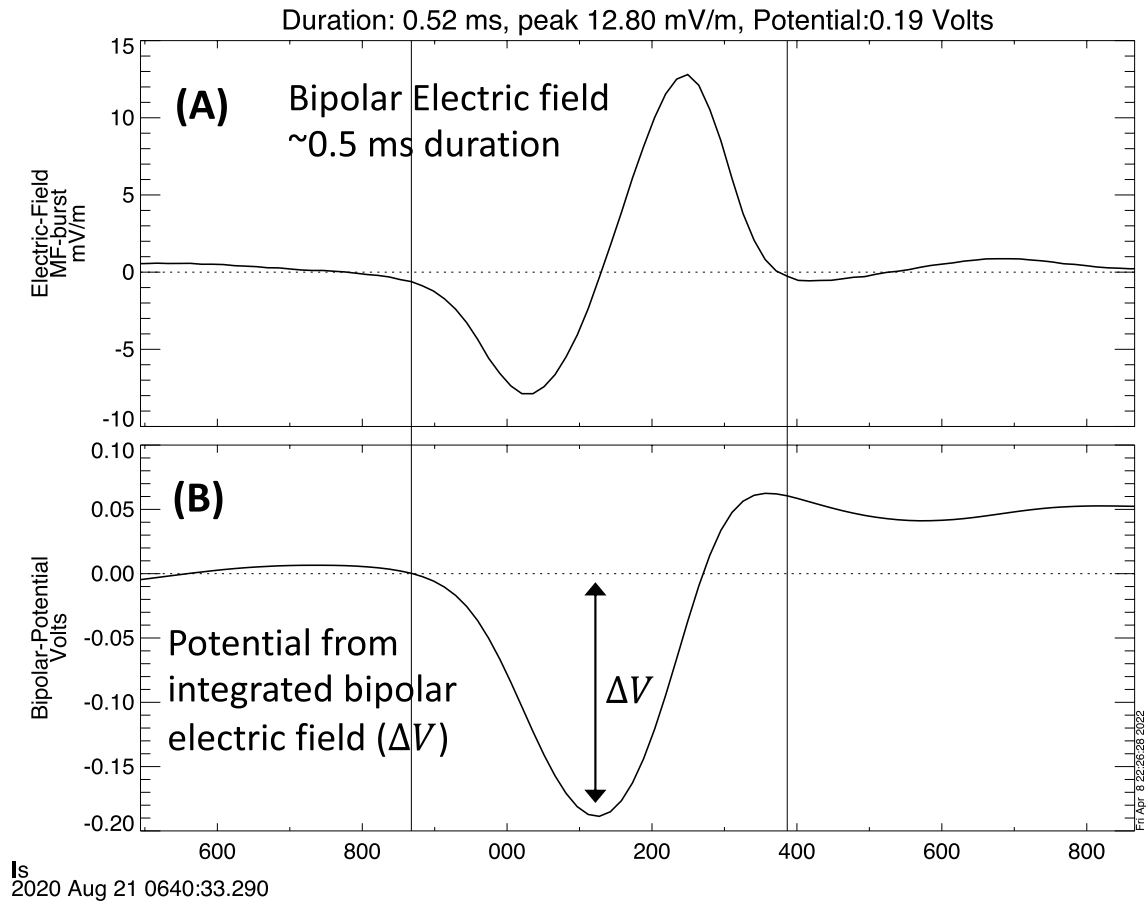
Figure 10. Example bipolar electric field (a) and corresponding potential found from integration of the electric field (b) assuming a speed of 5 Debye lengths/duration or $\sim 5 \times 10^5$ m/s. The gain curve correction has been applied. The pair of vertical lines mark the approximate start and end times of the structure. The arrow in (b) shows the potential difference being reported, the depth of the well from the structure start time to the midpoint where the electric field passes through zero.
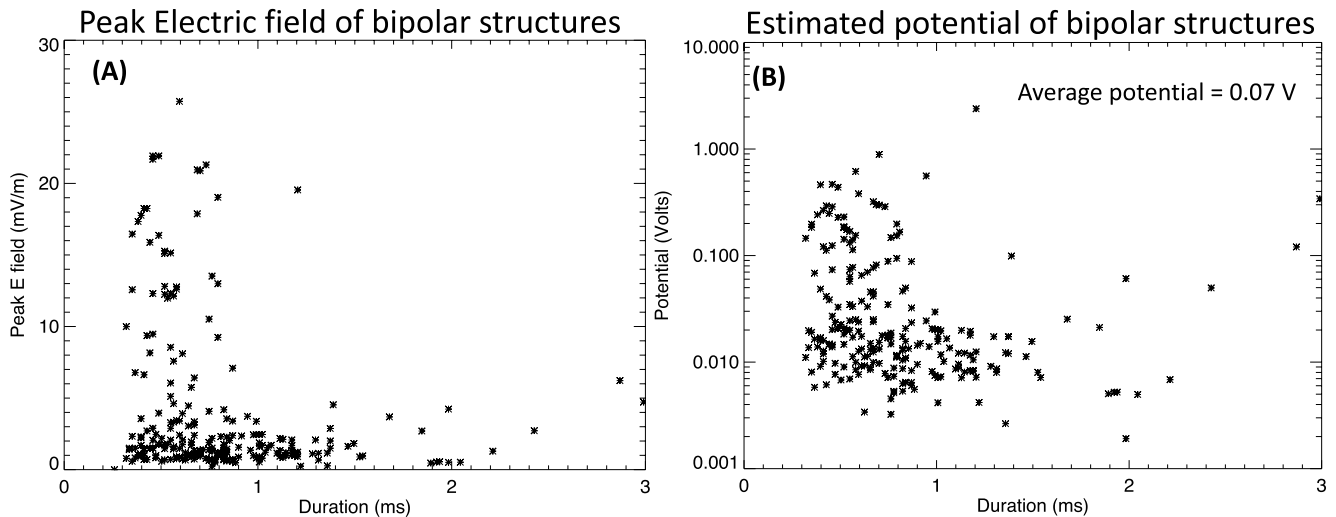
Figure 11. Statistical scatter of the peak bipolar electric field amplitude (with gain factor applied to the data) versus temporal duration of the bipolar structure are shown in panel (a). The estimated potential based on assuming a scale size of 5 Debye length and correcting for the angle between the probes and magnetic field is shown in panel (b).

structures is $\sim$0.07 V. If we apply a correction to account for the measured potentials being lower than the actual due to the finite separation of the Langmuir Probe sensors, we get an average potential of $\sim$0.08 V.

We note that the possibility that these bipolar structures are created by an ion streaming instability resulting from the ion beam in the frame of the solar wind described above, makes ion phase-space holes a likely candidate for these structures (e.g., Wang et al., 2021). If these structures are ion phase-space holes then their perpendicular scale size should be on the order of the thermal proton gyroradius (e.g., Wang et al., 2021), which for these observations are $\sim$200 km. In this case the approximation of spherical shape is not applicable, given the perpendicular size of $\sim$200 km and parallel size of $\sim$50 m (5 Debye lengths), and Equation 5 instead becomes $\int_0^\infty E_m v_{BP} dt = \Phi_0 \cos(\theta) 0.8 (1 + 0.0002\tan(\theta))$. The average, over the 235 bipolar fields used in this study, of $1 + 0.83\tan(\theta)$ is 3.6, and the average value for $1 + 0.0002\tan(\theta)$ is 1.0006. Thus, if the actual shape of the bipolar structures is pancake with a parallel to perpendicular scale ratio of 50 m/2,000,000 m, the average potential will be higher than the $\sim$0.07 eV estimated above by a factor of 3.6, it will instead be $\sim$0.25 V.

Using the average potential of $\sim$0.07 V, we can estimate the impact these bipolar electric field structures should have on the protons. In the relatively slow-moving spacecraft frame, we observe $\sim$100 burst captures containing bipolar fields per hour, an average rate of $\sim$0.028 s^{-1}. Some captures contain several such bipolar structures; so as not to underestimate the total rate, we multiply the bipolar field burst capture rate by 3 bipolar fields per burst capture for an estimated frequency of bipolar field observations of $\sim$0.083 s^{-1}. This frequency, f_{BP}, is related to the speed of these structures, v_{BP}, cross sectional area, $A_{BP} = \pi L_\perp^2 \approx \pi (2.5\lambda_{De})^2$, and density, n_{BP}, as $f_{BP} = n_{BP} A_{BP} v_{BP}$. To estimate the number of encounters a proton will have with bipolar field structures over one gyration, we multiply the proton gyro-period by the collision frequency between proton and bipolar structures, $f_{BPP} = n_{BP} A_{BP} |v_{BP} - v_p| = \left(\frac{f_{BP}}{v_{BP}}\right) |v_{BP} - v_p|$. The relevant speeds to consider are the speed of the bipolar structures $v_{BP} \sim$5 λ_{De}/0.5 ms $\sim$50 m/0.0005 s $\sim 1 \times 10^5$ m/s, and the proton thermal speed of $v_p \sim 6 \times 10^4$ m/s (for 40 eV). An upper limit for the magnitude of the velocity difference is thus $\sim 1.6 \times 10^5$ m/s. Using these numbers, we find that $f_{BPP} \sim 0.13$ s^{-1}. For a 5 nT field, a proton has a gyro-period of $\sim$13.3 s, and we can expect $\sim$1.73 collisions with bipolar field structures per gyration. Taking this encounter rate and the average potential of the structures of 0.07 V, the largest expected energy change per gyration is $\sim$0.07 V/collision $\times$ 1.73 collisions/gryration = 0.12 eV. Given the typical proton energy of 40 eV, this corresponds to a change in the energy of $\sim$0.3%. The change in the proton gyroradius per interaction with a bipolar structure will be $\sim$0.15%, or $\sim$0.28 km, which is small relative to the boundary thickness, $\sim$200 km, described in the introduction. In the time of one proton gyration, $\sim$13.3 s, the protons in the sheath flow, moving at $\sim$200 km/s, will be swept down the sheath anti-sunward by $\sim$2,660 km or $\sim$0.7 R$_M$. For the gyroradius to change by an amount of 10% of the system boundary thicknesses, or $\sim$20 km, the protons will have to gain $\sim$9 eV, which will require $\sim$129 collisions with bipolar structures. The time needed for 129 collision is 129 collision/0.13 collision per sec $\sim$990 s. In that time, the proton will be $\sim$58 R$_M$ down in the anti-sunward direction of Mars. If we use the average potential value of $\sim$0.08 V that compensates for the effects of the finite sensor separation described above, and then increase this by 3.6 in the case that they are pancake shape, we get an average potential of $\sim$0.29 V. An average potential of $\sim$0.29 V will mean the protons can gain or lose $\sim$0.5 eV per gyration, a change of $\sim$1.2%. Propagating this result, protons will increase their energy by 10% in 18 collisions, which will take 138 s, in which time the plasma moves $\sim$8 R$_M$. The interaction between the sheath protons and bipolar structures are thus expected to have minimal impact on the proton dynamics, under the assumption that the protons can gain an energy equal to the full drop of the bipolar structure's potential well depth.

It should be noted that direct energization by gaining the full energy associated with a displacement from the bipolar structure's center to the edge, along the parallel direction, is unlikely. A more likely scenario for energization would be that the electrostatic potential of these structures is asymmetric along the propagation direction, and charged particles that pass through them will gain or lose that energy. The potential structures observed do often appear asymmetric. However, this asymmetry may be an artifact of the fact that only one dimension of the electric field is being measured, and that being a convolution of components of the parallel and perpendicular fields. The superposition of the measured components, when the structure passes off-center over the spacecraft, can change in such a way to yield an asymmetric bipolar structure in the measurement, even if the bipolar structure is symmetric in reality. Since the net drops are smaller than the depth of the potential wells, by showing that even the full depth of the potential will not significantly energize protons in the Martian sheath, we can extend the conclusion to the more likely case of the smaller net potential drops.

The analysis presented above considers the potentials along the magnetic field. We can also consider how a bipolar structure with a large perpendicular scale length, for example, the pancake shaped ($L_\perp \gg L_\parallel$) structure describe above, may energize particles along the perpendicular electric field. As the bipolar structure passes over a gyrating proton, the proton will experience its perpendicular electric field for a duration dependent on the relative speed between the proton and bipolar field. Using the ~0.5 ms duration in the MAVEN frame, a 40 eV proton will move ~44 m in that time and could pick up or lose as much as 10 mV/m × 44 m, or ~0.44 eV, or ~1%. This would result in a ~2% change in energy per gyration. In the case of an electron, with a gyrofrequency of 140 Hz in the 5 nT field (the value used for the proton above), the electron will undergo 0.7 gyrations in the time it takes the bipolar structure to pass over it, again using 0.5 ms for the transit time. The gyroradius of a ~10 eV electron in a 5 nT field is ~2 km. Thus, an electron may gain or lose ~1,000 m × 10 mV/m ~ 10 eV, or undergo a change in energy of ~100% change. If this process is occurring, electrons may undergo significant energy change. However, since a ~10 eV electron moves at ~1.9 × 10⁶ m/s, almost ~20x the speed of the bipolar structures, the electrons are likely to experience the perpendicular electric field for a shorter duration of ~5 × 10 m/1.9 × 10⁶ m/s or 2.67 × 10⁻⁵ s. In this shorter time the electron will only move long its gyration ~50 m, and so end up with a smaller change of energy, ~0.5 eV, or ~5%, in a 10 mV/m field.

It should be further noted that we do not here consider other possible mechanism of particle energization that these bipolar structures may play a role in. Bipolar electrostatic solitary structures have been shown to be efficient at pitch angle scattering (Vasko et al., 2018). In addition, periods of strongly compressional, $\delta|B|/\overline{|B|} \sim 2$, waves are sometimes observed during the intervals in which the bipolar fields occur. The interaction between cyclic magnetic field compressions and pitch angle scattering can result in energization through magnetic pumping (Borovsky et al., 2017). Thus, it is possible that these bipolar structures play an important role in other, potentially significant, particle energization mechanisms.

We can estimate how far an individual bipolar structure may propagate in the sheath using the assumption that their propagation along the magnetic field is limited to the distance over which the magnetic field changes strongly. Since both acoustic solitary structures (e.g., Vasko et al., 2017) and phase space holes (e.g., Hutchinson, 2017) propagate along the background magnetic field, when changes in the background field are significant, distortion and dissipation of the bipolar structures are expected. One source of strong gradients in the magnetic field could be the strongly compressional, $\delta|B|/\overline{|B|} \sim 2$, waves that are occasionally seen in conjunction with the bipolar fields. These waves are highly steepened, as opposed to sinusoidal, and appear to be similar or related to those described by Fowler et al. (2019), Shan et al., (2020, 2020), and elsewhere. A typical time over which the magnetic field magnitude increases in the spacecraft frame is ~3 s. Since the flow speed, ~200 km/s, is super-Alfvenic (the Alfven speed being ~ 40 km/s), the magnetic field spatial gradient can be estimated by treating the wave perturbations as spatial structures being advected over MAVEN in the plasma flow. We estimate the spatial scale of the gradient as ~200 km/s × 3 s = 600 km. Estimating the speed of the bipolar structure as $5\lambda_{De}/\delta t$, where δt is the pulse duration of ~0.5 ms, and λ_{De} ~6–12 m, gives speeds of 60–120 km/s, in the spacecraft frame. This suggest the bipolar structures should last for ~600 km/(60–120 km/s) ~5–10 s. We note that the steepened compressive waves are not always observed in conjunction with the bipolar structures, and thus this estimate of the propagation distance applies only to a subset of the bipolar structures observed.

4. Conclusion

Bipolar electric fields of ~0.0003–0.001 s duration (in the spacecraft frame) and amplitudes ~1–25 mV/m are observed in the sheath and solar wind by the MAVEN LPW, appearing in the medium frequency burst waveform captures as Mars approaches perihelion in 2020. The occurrence of these bipolar structures is not unexpected as they are routinely observed in various locations in Earth's magnetosphere, bow shock, and upstream solar wind. In this study we estimate these bipolar electric fields to have a net potential drop of ~0.07 V (with a range of ~0.002 – ~2 V), ~0.08 V when the underestimate of the potential due to finite sensor separation is factored in. Given the observed occurrence rate of these bipolar structures and the sheath proton parameters, we estimate that the protons will at most change their energy by ~0.3% per gyration. At this rate the sheath flow will carry the plasma ~58 R_M anti-sunward before the proton gyroradius is changed by an amount of 10% of the boundary thicknesses. The average potential depth of the bipolar structures could be as deep as ~0.29 V factoring in the possibility of them being pancake-shaped ($L_\perp \gg L_\parallel$) and the underestimate of the potential due to the finite sensor separation. In the case of an average ~0.29 V potential, protons would gain or lose ~0.5 eV per gyration

(or ~1.2%), changing their energy by 10% in 18 collisions, which will take 138 s, in which time they will move ~8 R_M anti-sunward. Estimates of the energy change via interaction with the bipolar structure's perpendicular field yield similar results. Thus, the interaction between protons and the bipolar structures, via direct energization by the potential drop, should not play a significant role in modifying proton dynamics. However, other energization mechanism, such as magnetic pumping, may be important.

Data Availability Statement

MAVEN data is available online through the PDS and can be found at https://pds-ppi.igpp.ucla.edu/search/?t=Mars%26sc=MAVEN%26facet=SPACECRAFT_NAME%26depth=1. As well as at https://lasp.colorado.edu/maven/sdc/public/pages/datasets/lpw.html. The MAVEN project is supported by NASA through the Mars Exploration Program. Work at the Laboratory for Atmospheric and Space Physics was done under the MAVEN project.

References

Andersson, L., Ergun, R., Delory, G., Eriksson, A., Westfall, J., Reed, H., et al. (2015). The Langmuir probe and waves (LPW) instrument for MAVEN. *Space Science Reviews*, *195*(1–4), 173–198. https://doi.org/10.1007/s11214-015-0194-3

Andersson, L., Ergun, R. E., Tao, J., Roux, A., LeContel, O., Angelopoulos, V., et al. (2009). New features of electron phase space holes observed by the THEMIS mission. *Physical Review Letters*, *102*(22), 225004. (Published 5 June 2009). https://doi.org/10.1103/physrevlett.102.225004

Aravindakshan, H., Kakad, A., Kakad, B., & Yoon, P. H. (2021). Structural characteristics of ion holes in plasma. *Plasma*, *4*(3), 435–449. https://doi.org/10.3390/plasma4030032

Bale, S. D., Kellogg, P. J., Larsen, D. E., Lin, R. P., Goetz, K., & Lepping, R. P. (1998). Bipolar electrostatic structures in the shock transition region: Evidence of electron phase space holes. *Geophysical Research Letters*, *25*(15), 2929–2932. https://doi.org/10.1029/98gl02111

Berk, H. L., Nielsen, C. E., & Roberts, K. V. (1970). Phase space hydrodynamics of equivalent nonlinear systems: Experimental and computational observations. *The Physics of Fluids*, *13*(4), 980. https://doi.org/10.1063/1.1693039

Berthomier, M., Pottelette, R., Malingre, M., & Khotyaintsev, Y. (2000). Electron-acoustic solitons in an electron beam plasma system. *Physics of Plasmas*, *7*, 2987–2994. https://doi.org/10.1063/1.874150

Borovsky, J. E., Horne, R. B., & Meredith, N. P. (2017). The contribution of compressional magnetic pumping to the energization of the Earth's outer electron radiation belt during high-speed stream-driven storms. *Journal of Geophysical Research: Space Physics*, *122*(12), 12072–12089. https://doi.org/10.1002/2017JA024607

Cattell, C. A., Wygant, J., Dombeck, J., Mozer, F. S., Temerin, M., & Russell, C. T. (1998). Observations of large amplitude parallel electric field wave packets at the plasma sheet boundary. *Geophysical Research Letters*, *25*(6), 857–860. https://doi.org/10.1029/98gl00497

Connerney, J. E. P., Espley, J., Lawton, P., Murphy, S., Odom, J., Oliversen, R., et al. (2015). The MAVEN magnetic field investigation. *Space Science Reviews*, *195*(1–4), 257–291. https://doi.org/10.1007/s11214-015-0169-4

Crumley, J. P., Cattell, C. A., Lysak, R. L., & Dombeck, J. P. (2001). Studies of ion solitary waves using simulations including hydrogen and oxygen beams. *Journal of Geophysical Research*, *106*(A4), 6007–6015. https://doi.org/10.1029/2000JA003038

Dombeck, J. C., Cattell, C., Crumley, J., Peterson, W. K., Collin, H. L., & Kletzing, C. (2001). Observed trends in auroral zone ion-mode solitary wave structure characteristics using data from Polar. *Journal of Geophysical Research*, *106*(A9), 19013–19021. https://doi.org/10.1029/2000ja000355

Dong, Y., Fang, X., Brain, D. A., McFadden, J. P., Halekas, J. S., Connerney, J. E., et al. (2015). Strong plume fluxes at Mars observed by MAVEN: An important planetary ion escape channel. *Geophysical Research Letters*, *42*(21), 8942–8950. https://doi.org/10.1002/2015GL065346

Fowler, C. M., Halekas, J., Schwartz, S., Goodrich, K. A., Gruesbeck, J. R., & Benna, M. (2019). The modulation of solar wind hydrogen deposition in the Martian atmosphere by foreshock phenomena. *Journal of Geophysical Research: Space Physics*, *124*(8), 7086–7097. https://doi.org/10.1029/2019JA026938

Franz, J. R., Kintner, P. M., Pickett, J. S., & Chen, L. J. (2005). Properties of small-amplitude electron phase-space holes observed by Polar. *Journal of Geophysical Research*, *110*(A9), A09212. https://doi.org/10.1029/2005JA011095

Fuselier, S. A., Gary, S. P., Thomsen, M. F., Bame, S. J., & Gurnett, D. A. (1987). Ion beams and the ion/ion acoustic instability upstream from the Earth's bow shock. *Journal of Geophysical Research*, *92*(A5), 4740–4744. https://doi.org/10.1029/JA092iA05p04740

Gary, S. P. (1991). Electromagnetic ion/ion instabilities and their consequences in space plasmas: A review. *Space Science Reviews*, *56*(3–4), 373–415. https://doi.org/10.1007/BF00196632

Grard, R., Nairn, C., Pedersen, A., Klimov, S., Savin, S., Skalsky, A., & Trotignon, J. (1991). Plasma and waves around Mars. *Planetary and Space Science*, *39*(½), 89–98. https://doi.org/10.1016/0032-0633(91)90131-s

Halekas, J. S. (2017). Seasonal variability of the hydrogen exosphere of Mars. *Journal of Geophysical Research: Planets*, *122*(5), 901–911. https://doi.org/10.1002/2017JE005306

Halekas, J. S., Taylor, E. R., Dalton, G., Johnson, G., Curtis, D. W., McFadden, J. P., et al. (2015). The solar wind ion analyzer for MAVEN. *Space Science Reviews*, *195*(1–4), 125–151. https://doi.org/10.1007/s11214-013-0029-z

Hobara, Y., Walker, S. N., Balikhin, M., Pokhotelov, O. A., Gedalin, M., Krasnoselskikh, V., et al. (2008). Cluster observations of electrostatic solitary waves near the Earth's bow shock. *Journal of Geophysical Research*, *113*(A5), A05211. https://doi.org/10.1029/2007JA012789

Holmberg, M. K. G., André, N., Garnier, P., Modolo, R., Andersson, L., Halekas, J., et al. (2019). MAVEN and MEX multi-instrument study of the dayside of the Martian induced magnetospheric structure revealed by pressure analyses. *Journal of Geophysical Research: Space Physics*, *124*(11), 8564–8589. https://doi.org/10.1029/2019JA026954

Holmes, J. C., Ergun, R. E., Newman, D. L., Ahmadi, N., Andersson, L., LeContel, O., et al. (2018). Electron phase-space holes in three dimensions: Multispacecraft observations by magnetospheric multiscale. *Journal of Geophysical Research: Space Physics*, *123*(12), 9963–9978. https://doi.org/10.1029/2018JA025750

Hutchinson, I. H. (2017). Electron holes in phase space: What they are and why they matter. *Physics of Plasmas*, *24*(5), 055601. https://doi.org/10.1063/1.4976854

Jakosky, B. M., Lin, R. P., Grebowsky, J. M., Luhmann, J. G., Mitchell, D., Beutelschies, G., et al. (2015). The Mars atmosphere and volatile evolution (MAVEN) mission. *Space Science Reviews*, *195*(1–4), 3–48. https://doi.org/10.1007/s11214-015-0139-x

Khotyaintsev, Y. V., Vaivads, A., André, M., Fujimoto, M., Retino, A., & Owen, C. J. (2010). Observations of slow electron holes at a magnetic reconnection site. *Physical Review Letters*, *105*(16), 165002. https://doi.org/10.1103/physrevlett.105.165002

Lefebvre, B., Chen, L.-J., Walter, G., Paul, K., Pickett, J., Pribyl, P., et al. (2010). Laboratory measurements of electrostatic solitary structures generated by beam injection. *Physical Review Letters*, *105*(11), 115001. (Published 7 September 2010). https://doi.org/10.1103/physrevlett.105.115001

Lotko, W., & Kennel, C. (1983). Spiky ion acoustic waves in collisionless auroral plasma. *Journal of Geophysical Research*, *88*(A1), 381. https://doi.org/10.1029/ja088ia01p00381

Lynov, J. P., Michelsen, P., Pécseli, H. L., Juul Rasmussen, K. S. J., Saeki, K., & Turikov, V. A. (1979). Observations of solitary structures in a magnetized plasma loaded wave guide. *Physica Scripta*, *20*(3–4), 328–335. https://doi.org/10.1088/0031-8949/20/3-4/005

Main, D. S., Newman, D. L., & Ergun, R. E. (2006). Double layers and ion phase-space holes in the auroral upward-current region. *Physical Review Letters*, *97*, 185001. https://doi.org/10.1103/PhysRevLett.97.185001

Mazelle, C., Winterhalter, D., Sauer, K., Trotignon, J., Acuna, M., Baumgartel, K., et al. (2004). Bow shock and upstream phenomena at Mars. *Space Science Reviews*, *111*(1/2), 115–181. https://doi.org/10.1023/B:SPAC.0000032717.98679.d0

McFadden, J., Kortmann, O., Curtis, D., Dalton, G., Johnson, G., Abiad, R., et al. (2015). MAVEN suprathermal and thermal ion composition (STATIC) instrument. *Space Science Reviews*, *195*(1–4), 199–256. https://doi.org/10.1007/s11214-015-0175-6

Mitchell, D. L., Mazelle, C., Sauvaud, J. A., Thocaven, J.-J., Rouzaud, J., Fedorov, A., et al. (2016). The MAVEN solar wind electron analyzer. *Space Science Reviews*, *200*(1), 495–528. https://doi.org/10.1007/s11214-015-0232-1

Morse, R. L., & Nielson, C. W. (1969). Numerical simulation of warm two-beam plasma. *The Physics of Fluids*, *12*(11), 2418. https://doi.org/10.1063/1.1692361

Nairn, C., Grard, R., Skalsky, A., & Trotignon, J. (1991). Waves and cold plasma observations near mars. *Advances in Space Research*, *11*(9), 87–91. https://doi.org/10.1016/0273-1177(91)90017-e

Saeki, K., Michelsen, P., Pdcseli, H. L., & Juul Rasmussen, J. (1979). Formation and coalescence of electron solitary holes. *Physical Review Letters*, *42*(8), 501–504. https://doi.org/10.1103/physrevlett.42.501

Sauer, & Dubinin (2004). Multi-ion space plasma research: Beam-driven oscillitons as origin of coherent waves and gyrating ions. *Physica Scripta*, 167.

Schamel, H. (1986). Electron holes, ion holes and double layers: Electrostatic phase space structures in theory and experiment. *Physics Reports*, *140*(3), 161–191. ISSN 0370-1573. https://doi.org/10.1016/0370-1573(86)90043-8

Shan, L., Du, A., Tsurutani, B. T., Ge, Y. S., Lu, Q., Mazelle, C., et al. (2020). In situ observations of the formation of periodic collisionless plasma shocks from fast mode waves. *The Astrophysical Journal Letters*, *888*(2), L17. https://doi.org/10.3847/2041-8213/ab5db3

Shan, L., Tsurutani, B. T., Ohsawa, Y., Mazelle, C., Huang, C., Du, A., et al. (2020). Observational evidence for fast mode periodic small-scale shocks: A new type of plasma phenomenon. *The Astrophysical Journal Letters*, *905*(L4), 6. https://doi.org/10.3847/2041-8213/abcb02

Stone, R. (1991). Some average distance results. *Transportation Science*, *25*(1).

Trotignon, J. G., Mazelle, C., Bertucci, C., & Acuña, M. H. (2006). Martian shock and magnetic pile-up boundary positions and shapes determined from the Phobos 2 and Mars Global Surveyor data sets. *Planetary and Space Science*, *54*(4), 357–369. https://doi.org/10.1016/j.pss.2006.01.003

Vasko, I. Y., Agapitov, O. V., Mozer, F. S., Bonnell, J. W., Artemyev, A. V., Krasnoselskikh, V. V., et al. (2017). Electron-acoustic solitons and double layers in the inner magnetosphere. *Geophysical Research Letters*, *44*(10), 4575–4583. https://doi.org/10.1002/2017GL074026

Vasko, I. Y., Mozer, F. S., Krasnoselskikh, V. V., Artemyev, A. V., Agapitov, O. V., Bale, S. D., et al. (2018). Solitary waves across supercritical quasi-perpendicular shocks. *Geophysical Research Letters*, *45*, 5809–5817. https://doi.org/10.1029/2018GL077835

Vignes, D., Mazelle, C., Rme, H., Acuña, M. H., Connerney, J. E. P., Lin, R. P., et al. (2000). The solar wind interaction with Mars: Locations and shapes of the bow shock and the magnetic pile-up boundary from the observations of the MAG/ER Experiment onboard Mars Global Surveyor. *Geophysical Research Letters*, *27*(1), 49–52. https://doi.org/10.1029/1999gl010703

Wang, R., Vasko, I. Y., Mozer, F. S., Bale, S. D., Kuzichev, I. V., Artemyev, A. V., et al. (2021). Electrostatic solitary waves in the Earth's bow shock: Nature, properties, lifetimes, and origin. *Journal of Geophysical Research: Space Physics*, *126*(7), e2021JA029357. https://doi.org/10.1029/2021JA029357

Xu, S., Liemohn, M. W., Dong, C., Mitchell, D. L., Bougher, S. W., & Ma, Y. (2016). Pressure and ion composition boundaries at Mars. *Journal of Geophysical Research: Space Physics*, *121*(7), 6417–6429. https://doi.org/10.1002/2016JA022644

Yamauchi, M., Hara, T., Lundin, R., Dubinin, E., Fedorov, A., Sauvaud, J.-A., et al. (2015). Seasonal variation of Martian pick-up ions: Evidence of breathing exosphere. *Planetary and Space Science*, *119*, 54–61. https://doi.org/10.1016/j.pss.2015.09.013